Supplemental Material: Resonant and Bound States of Charged Defects in Two-Dimensional Semiconductors

Martik Aghajanian,[1] Bruno Schuler,[2,*] Katherine A. Cochrane,[2] Jun-Ho Lee,[2,3] Christoph Kastl,[2,4] Jeffrey B. Neaton,[2,3,5] Alexander Weber-Bargioni,[2] Arash A. Mostofi,[1] and Johannes Lischner[1,†]

[1]*Departments of Physics and Materials and the Thomas Young Centre for Theory and Simulation of Materials, Imperial College London, London, SW7 2AZ, UK.*

[2]*Molecular Foundry, Lawrence Berkeley National Laboratory, Berkeley, California 94720, USA.*

[3]*Department of Physics, University of California at Berkeley, Berkeley, California 94720, USA.*

[4]*Walter-Schottky-Institut and Physik-Department, Technical University of Munich, Garching 85748, Germany.*

[5]*Kavli Energy Nanosciences Institute at Berkeley, Berkeley, California 94720, USA.*

CONTENTS

CALCULATION OF THE SCREENED DEFECT POTENTIAL

The screened defect potential is obtained by dividing the bare Coulomb potential by the dielectric function in the random phase approximation (RPA) given by

$$\varepsilon_{\mathrm{RPA}}(q) = -v(q)\left[\chi_{\mathrm{TMD}}(q) + e^{-z_{\mathrm{g}}q}\chi_{\mathrm{Gr}}(q)\right] + \eta(q), \tag{S1}$$

where $v(q) = 2\pi e^2/q$ denotes the 2D Fourier transform of the Coulomb interaction. The dielectric function of Eq.(S1) is a sum of three contributions. The first term on the right hand side describes screening from the TMD, with $\chi_{\mathrm{TMD}}(q)$ denoting the polarizability of WS_2 obtained from first-principles calculations based on the Adler-Wiser formula[1]. The second term captures the screening from the doped graphene monolayer that sits a distance $z_{\mathrm{g}} = 4.9$ Å beneath the TMD (measured from the plane of the transition metal atoms). The value of z_{g} was obtained from density-functional theory (DFT) calculations including van der Waals interactions. Specifically, $\chi_{\mathrm{Gr}}(q)$ is the RPA polarizability of doped graphene given by[2]

$$\chi_{\mathrm{Gr}}(q) = -\frac{2k_{\mathrm{F}}}{\pi\hbar v_{\mathrm{F}}}\left[1 - \Theta(q-2k_{\mathrm{F}})\Lambda(q)\right], \tag{S2}$$

$$\Lambda(q) = \frac{1}{2}\sqrt{1-\left(\frac{2k_{\mathrm{F}}}{q}\right)^2} - \frac{q}{4k_{\mathrm{F}}}\cos^{-1}\left(\frac{2k_{\mathrm{F}}}{q}\right), \tag{S3}$$

where k_{F} and v_{F} denote the Fermi wavevector and Fermi velocity of the doped graphene, respectively. We use $v_{\mathrm{F}} = 1.15\times10^6$ ms^{-1}[3] and $k_{\mathrm{F}} = 0.059$ Å^{-1}[4]. Finally, the last term in Eq. (S1) describes the screening by the SiC substrate located a distance $z_{\mathrm{s}} = 1.7$ Å beneath the graphene layer[5]. An image charge model yields

$$\eta(q) = \frac{\varepsilon_{\mathrm{SiC}}+1}{\varepsilon_{\mathrm{SiC}}+1-(\varepsilon_{\mathrm{SiC}}-1)e^{-2q(z_{\mathrm{s}}+z_{\mathrm{g}})}}, \tag{S4}$$

with $\varepsilon_{\mathrm{SiC}} = 9.7$ denoting the bulk dielectric constant of SiC[6].

The defect potential in real space is obtained via a Hankel transform[7]

$$V(r) = Ze^2\int \mathrm{d}q\, \frac{e^{-qz_{\mathrm{d}}}J_0(qr)}{\varepsilon_{\mathrm{RPA}}(q)}, \tag{S5}$$

where Z and z_{d} denote the defect charge and the distance of the defect above the transition-metal plane, respectively. We assume a defect charge of $Z = -1$ and use $z_{\mathrm{d}} = 2.4$ Å. We note that z_{d} should not be interpreted as the actual defect height. Instead, this parameter regularizes the Coulomb interaction at short distances and reflects the central cell correction that is required to

capture chemical effects close to the impurity[8]. We have carried out calculations for different values z_{d} and determined that 2 Å gives the best agreement with experiment for the LDOS.

To obtain the dielectric function of WS_2 within the random-phase approximation, we first perform density-functional theory (DFT) calculations of a structurally relaxed ($a_{\mathrm{lat}} = 3.19$ Å) monolayer of WS_2 using the PBE exchange-correlation functional with a plane-wave cut-off of 80 Ry and a $12\times12\times1$ k-point mesh as implemented in the Quantum Espresso software package[9]. To prevent interactions between periodically repeated monolayers, we employ a separation in the out-of-plane direction of $L_z = 18$ Å. We then calculate 2900 conduction band states on a finer $30 \times 30 \times 1$ k-point mesh, and utilise the BerkeleyGW package[10] to determine the inverse dielectric matrix $\varepsilon^{-1}_{\mathbf{GG'}}(\mathbf{q})$, using a truncated reciprocal-space Coulomb interaction $V_{\mathrm{trunc}}(\mathbf{q})$[11]. From this we extract an effective two-dimensional dielectric function of the TMD monolayer using[1]

$$\varepsilon^{-1}_{\mathrm{TMD}}(\mathbf{q}) = \frac{q}{2\pi e^2 L_z} \sum_{\mathbf{G}_z\mathbf{G}'_z} W_{\mathbf{G_z}\mathbf{G}'_{\mathbf{z}}}(\mathbf{q}), \tag{S6}$$

where $W_{\mathbf{G_z}\mathbf{G}'_{\mathbf{z}}}(\mathbf{q}) = \varepsilon^{-1}_{\mathbf{G_z}\mathbf{G}'_{\mathbf{z}}}(\mathbf{q}) V_{\mathrm{trunc}}(\mathbf{q} + \mathbf{G}'_{\mathbf{z}})$ denotes the screened interaction. We define the polarization function $\chi_{\mathrm{TMD}}(\mathbf{q})$ via the expression $\varepsilon_{\mathrm{TMD}}(\mathbf{q}) = 1 - v(\mathbf{q})\chi_{\mathrm{TMD}}(\mathbf{q})$, where $v(\mathbf{q})$ is the 2D Fourier transform of the bare Coulomb potential.

DETERMINATION OF z_{g}

To obtain a value for z_{g}, the distance between the WS_2 and the graphene, we carried out DFT calculations including van der Waals (vdW) interactions. Specifically, we studied a supercell that contains $4 \times 4 = 16$ unit cells of WS_2 on top of $5 \times 5 = 25$ unit cells of graphene. A $5 \times 5 \times 1$ k-point mesh was used. To deal with the lattice mismatch between graphene and WS_2, we applied 2.13% in-plane compressive strain to the WS_2. In order to take vdW interactions into account, we used the rev-vdW-DF2 scheme[12] that accurately describes the geometry of layered materials[13]. To determine the value of z_{g}, we averaged over the z-coordinates of the C and W atoms in the supercell.

DETERMINATION OF $z_{\mathbf{d}}$

We have carried out calculations of the defect binding energies for various values of the parameter z_{d}, which formally can be interpreted as the height of the defect above the plane of the

transition metal atoms. Our results are shown in Fig. S1. As z_d increases, the potential experienced by the electrons in the WS_2 is weaker resulting in smaller binding energies. The $1s$ states are more sensitive to changes in z_d than the $2p$ states as the most significant changes to the potential occur in the WS_2 region underneath the defect where the $2p$ states have a node (note that the hybridization of the localized $2p$ state from the Γ valley with the continuum states from the K/K′ valleys gives rise to multiple mixed states with are labelled by $2p_n(\Gamma)$ in Fig. S1). As a consequence of the larger effective mass of the Γ valley, the $1s(\Gamma)$ state is more localized than the $1s$(K/K′) state and therefore decreases more quickly as z_d is increased. For a value of $z_\mathrm{d} = 2$ Å, the separation between $1s$(K/K′) and $1s(\Gamma)$ is about 0.1 eV and the separation between $1s$(K/K′) and $2p(\Gamma)$ is about 0.3 eV in agreement with the separation of the experimentally measured binding energy differences (see below).

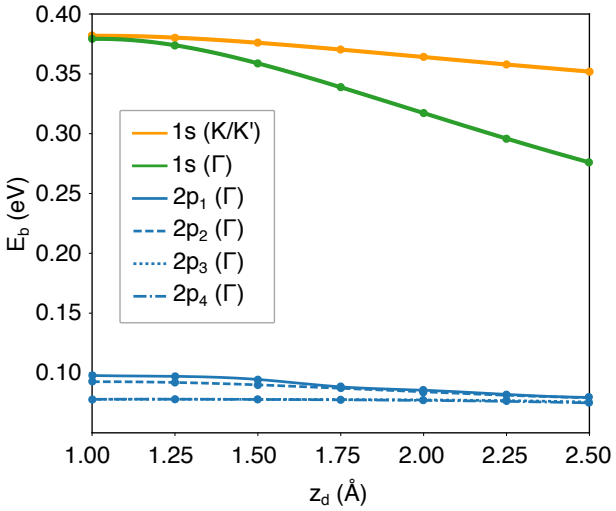

Figure S1. Dependence of the binding energy (measured with respect to the secondary valence band maximum at Γ) of various defect states on the parameter z_d.

CHEMICAL ORIGIN OF CHARGED DEFECTS

We frequently observe negatively charged defects in CVD-grown WS_2 as well as in MOCVD-grown WSe_2. We attribute these defects to acceptor-like impurities in the TMD crystal. Using CO-tip noncontact AFM we find that the negatively charged defects are centered on sulfur sites[14]. Two candidates are plausible that are consistent with all experimental evidence and synthetic conditions: CH substituting S (CH_S) or N substituting S (N_S). Both types of impurity defects

introduce formally unoccupied defect states close to (in the case of N_S) or in the valence band (in the case of CH_S) as shown in the DFT calcuted band structure in Fig. S2.

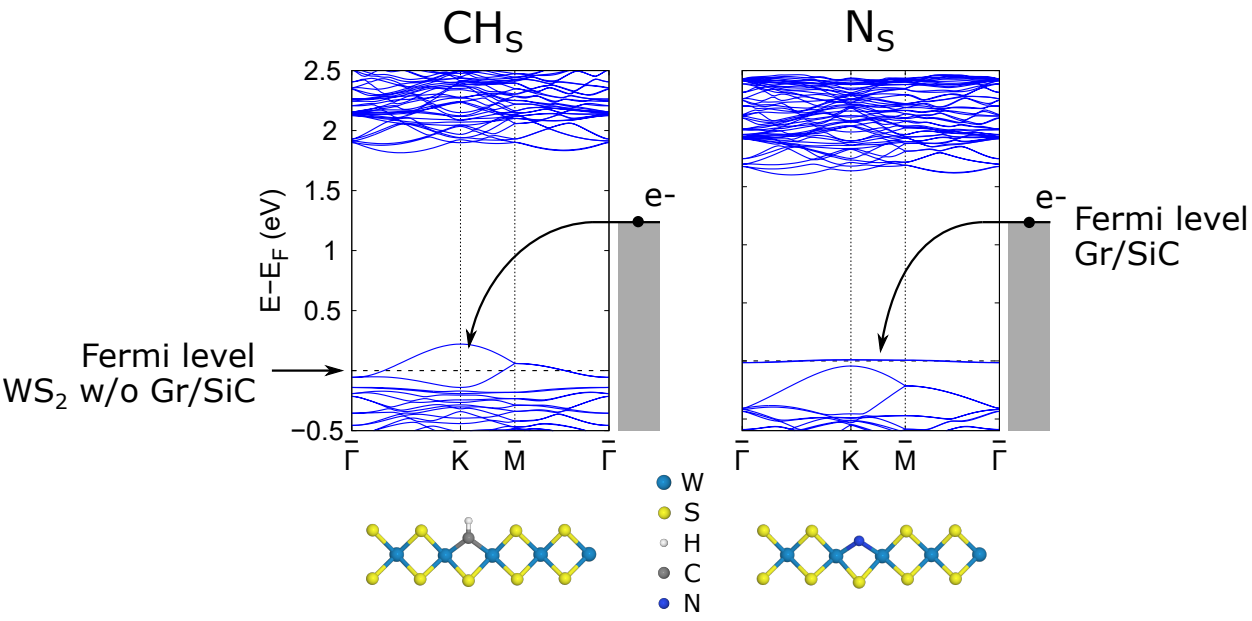

Figure S2. DFT calculated band structure of CH (left) and N substituting a S atom. The horizontal dashed line indicates the Fermi level of an isolated slab of WS_2. Both types of defects feature formally unoccupied states in the valence band (for CH_S) or in the band gap in the vicinity of the valence band maximum (for N_S). The graphene/SiC substrate pins the Fermi level of the heterostructure to the upper half of the WS_2 band gap (gray bar to the right of each band structure), hence filling the empty defect states, resulting in a net negatively charged defect.

Since the TMD is in electrical contact with the graphene/SiC substrate, which pins the Fermi level to the upper half of the WS_2 band gap, the formally unoccupied defect states are filled (black arrows in Fig. S2). Hence, the defects become negatively charged. Importantly, the hydrogenic states associated with such defects are largely independent of their actual chemical origin. However, the binding energies of the hydrogenic states depend on the defect charge and defect location, which are both known from experiment.

STM/STS MEASUREMENT PARAMETERS

STM/STS measurements were performed using a Createc scanning probe microscope under ultrahigh vacuum ($< 2\times10^{-10}$ mbar) at low temperature ($\sim$6 K) with a Au terminated tip verified

as metallic on a bare Au(111) substrate. All STS measurements were taken at constant height using a lock-in amplifier with a modulation frequency of 683 Hz and amplitudes between 2 mV for point spectra and 10 mV for maps.

EXPERIMENTAL BINDING ENERGIES

The binding energies of electronic resonances A, B, and C were determined from the tunneling spectra. Since the K band onset is difficult to observe unless at very close tip-sample separations, the Γ band was used as a reference. The Γ onset was determined by linear extrapolation of zero crossing (see red lines in fig S3). The energy difference between the K band and the Γ band of 240 meV, as determined previously from ARPES measurements,[15] was used to determine the onset of the K band. Binding energies were calculated as the difference between resonance peaks and the valence band onset. The values are given in the table of the main manuscript.

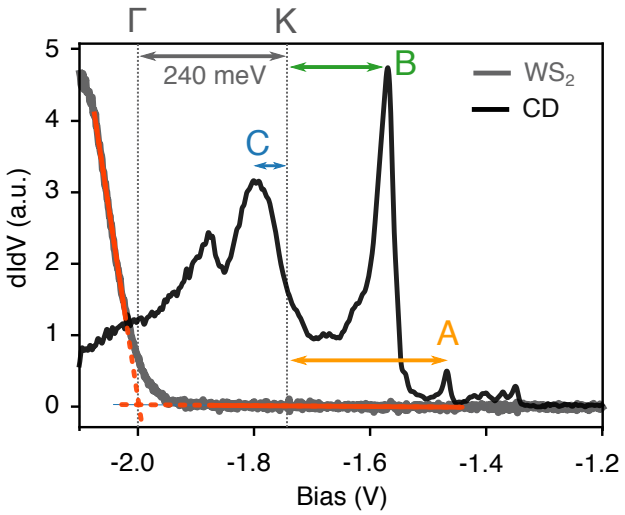

Figure S3. Determination of the experimental binding energies of states A, B and C. Red lines indicate linear fits used to extrapolate the Γ band onset from the WS_2 spectrum (gray). Yellow, green, and blue arrows indicate the binding energy with respect to the K band of the A, B, and C resonance respectively.

ADDITIONAL RESONANCES OBSERVED IN THE BAND GAP

In addition to the bound and resonance states A, B and C, there are four weak additional resonances observed just above state A, as shown in fig. S4. The origin of these states is currently

unclear.

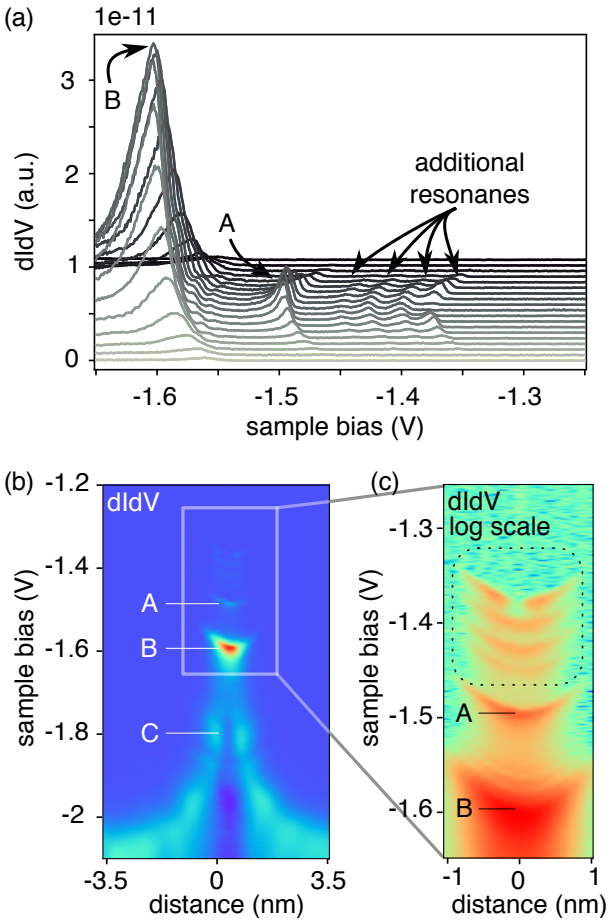

Figure S4. Scanning tunneling spectroscopy measurements of the charged defect showing the additional resonances above A. (a) Waterfall plot of constant height tunneling spectra taken along a line of a CD with states A and B labeled as well as the additional resonances observed between -1.35 V and -1.45 V. (b,c) Corresponding $\mathrm{d}I/\mathrm{d}V$ maps spatially resolving the additional states. Logarithmic color scale $\mathrm{d}I/\mathrm{d}V$ enhances the contrast of the states which are outlined with a black dotted box as shown in (c).

SIMULATED STM IMAGES

To calculate the spatial STS signatures of the resonant impurity states, we note that their components exhibit very different tunnelling matrix elements. In particular, the large in-plane momentum of the continuum states at K results in a short out-of-plane decay length and small tunnelling matrix element. In contrast, the contributions to the resonant impurity states from the Γ valley are expected to have a much larger tunnelling matrix element. As a first approximation,

we can therefore construct the STS image of a resonant defect state simply by neglecting the contribution of the continuum states from the K valley.

---

* bschuler@lbl.gov

† j.lischner@imperial.ac.uk

[1] D. Y. Qiu, F. H. da Jornada, and S. G. Louie, Phys. Rev. B **93**, 235435 (2016).

[2] B. Wunsch, T. Stauber, F. Sols, and F. Guinea, New Journal of Physics **8**, 318 (2006).

[3] C. Hwang, D. A. Siegel, S. Mo, W. Regan, A. Ismach, Y. Zhang, A. Zettl, and A. Lanzara, Sci. Rep. **2** (2012).

[4] K. V. Emtsev, A. Bostwick, K. Horn, J. Jobst, G. L. Kellogg, L. Ley, J. L. McChesney, T. Ohta, S. A. Reshanov, J. Röhrl, E. Rotenberg, A. K. Schmid, D. Waldmann, H. B. Weber, and T. Seyller, Nature Materials **8**, 203 (2009).

[5] T. L. Yoon, T. L. Lim, T. K. Min, S. H. Hung, N. Jakse, and S. K. Lai, **204702**, 1 (2013).

[6] L. Patrick and W. Choyke, Physical Review B **2**, 2255 (1970).

[7] M. Aghajanian, A. A. Mostofi, and J. Lischner, Scientific Reports **6**, 1 (2018).

[8] F. Bassani, G. Iadonisi, and B. Preziosi, Reports on Progress in Physics **37**, 1099 (1974).

[9] P. Giannozzi, S. Baroni, N. Bonini, M. Calandra, R. Car, C. Cavazzoni, D. Ceresoli, G. L. Chiarotti, M. Cococcioni, I. Dabo, *et al.*, Journal of physics: Condensed matter **21**, 395502 (2009).

[10] J. Deslippe, G. Samsonidze, D. A. Strubbe, M. Jain, M. L. Cohen, and S. G. Louie, Computer Physics Communications **183**, 1269 (2012).

[11] S. Ismail-Beigi, Physical Review B **73**, 233103 (2006).

[12] I. Hamada, Phys. Rev. B **89**, 121103(R) (2014).

[13] H. J. Kim, S. H. Kang, I. Hamada, and Y. W. Son, Phys. Rev. B **95**, 180101 (2017).

[14] B. Schuler, J.-H. Lee, C. Kastl, K. A. Cochrane, C. T. Chen, S. Refaely-Abramson, S. Yuan, E. van Veen, R. Roldan, N. J. Borys, *et al.*, ACS nano **13**, 10520 (2019).

[15] C. Kastl, C. Chen, R. J. Koch, B. Schuler, T. Kuykendall, A. Bostwick, C. Jozwiak, T. Seyller, E. Rotenberg, A. Weber-Bargioni, *et al.*, 2D Mater. **5**, 045010 (2018).